Natural statistics of human head orientation constrain models of vestibular processing

Supplementary material

Christian B. Sinnott[1,*], Peter A. Hausamann[2], and Paul R. MacNeilage[1]

[1]University of Nevada, Department of Psychology, Reno, 89557, United States of America
[2]Technical University of Munich, Department of Electrical and Computer Engineering, Munich, 80333, Germany
[*]csinnott@nevada.unr.edu

Bayesian model of perception of head orientation

Bayes' theorem states that the conditional probability of an event x given event y (posterior distribution) is equal to the product of the conditional probability of y given x (likelihood) and the probability of event x (prior), divided by the probability of event y (marginal).

$$P(x|y) = \frac{P(y|x)P(x)}{P(y)} \tag{1}$$

To model orientation perception, we substitute θ for x:

$$P(\theta|y) = \frac{P(y|\theta)P(\theta)}{P(y)} \tag{2}$$

$P(\theta)$ represents the prior probability across head orientation values based on the organism's prior experience. $P(y|\theta)$ is the likelihood, that is the probability of the current sensory information y given true head orientation θ. The posterior distribution $P(\theta|y)$ governs the perceptual estimate resulting from the model. It represents the conditional probability of true head orientation θ given current sensory information y. The marginal distribution in the denominator, $P(y)$, only serves to scale the product of the prior and likelihood distributions[1], so the equation can be simplified to:

$$P(\theta|y) \propto P(y|\theta)P(\theta) \tag{3}$$

In Eq. 3, the posterior distribution is proportional to the product of the likelihood and prior distributions. Our priors for head pitch and head roll models are kernel density estimates (KDEs) generated using our observed head pitch and head roll data. KDEs were generated using the `gaussian_kde` function in the `scipy.stats` library. Kernel bandwidth was determined using Scott's rule[2].

In addition to these empirical priors, we also model the likekihood. Previous work shows increased variability of perceptual estimates as head orientation eccentricity increases, presumably due to vestibular sensory noise that increases with tilt angle. We model this noise on the likelihood in two ways.

$$f(\alpha, \sigma, \theta) = \alpha + \sigma \times |\theta| \tag{4}$$

The first is through a linear increase in noise as orientation eccentricity increases, shown in Eq. (4). Alpha is a constant representing a baseline level of noise determined from previous research[3,4], while sigma is a Weber fraction denoting the proportion of signal dependent noise. Alpha is added to the product of sigma and the absolute value of theta; the orientation angle. Second, we increase noise with eccentricity non-linearly by using a sinusoidal function and incorporating two constants, G and K, to better simulate the effect of utricular shear experienced during linear acceleration of the head[5] (Eq. (5)).

$$f(\alpha, \sigma, sin(\theta), K, G) = \alpha + \sigma \times K \times G \times sin(|\theta|) \tag{5}$$

Alpha, sigma, and theta are the same terms here as they are in the linear noise model. G represents the constant linear acceleration imparted by gravity, while K is a scaling constant determined in previous research[5]. We use both these equations to apply noise to the likelihood distribution used in each of our models.

To generate model predictions for each value of sigma and each tilt angle, we take the mean of the posterior distribution where the posterior is calculated as the product of the noisy likelihood function (with noise determined by σ and Eq. (4) and (5)) and our empirical prior, according to Bayes' theorem (Eq. (3)).

Both of our models only contain one free parameter which is the level of signal dependent noise denoted by σ. Both linear and utricular shear models are first fit to extant psychophysical data observing bias in roll perception[4] by selecting the sigma value that minimizes distance between the observed error from psychophysical data and predicted error from the model. We repeat the same process using pitch perception data[6]. Our metric for distance is residual square error (RSE), calculated as:

$$RSE = \sqrt{\frac{1}{n-2}\sum_{i=1}^{n}(y_i - \hat{y}_1)^2} \tag{6}$$

Gravitational and inertial acceleration power spectra

After data were separated into separate high- and low-velocity epochs, we conducted power spectra analyses on both sets of epochs. Like before, crossing points were observed along all three axes, though the exact point of these crossing points differed from crossing points observed across all data. During low-velocity epochs, we observed crossing points at approximately 1.455 Hz (Fig. S1a), 0.77 Hz (Fig. S1b), and 0.758 Hz (Fig. S1c) along X-, Y-, and Z-axes, respectively. During high-velocity epochs, we observed crossing points at approximately 1.101 Hz (Fig. S2a), 0.566 Hz (Fig. S2b), and 0.525 Hz (Fig. S2c) along X-, Y-, and Z-axes. Additionally, power spectra estimated during high-velocity epochs showed a number of transient peaks through the frequency space along all axes, with a notable peak at approximately 2 Hz along X- and Z-axes corresponding with preferred stepping frequency[7]. No similar peaks were observed in the power spectra estimated during low-velocity epochs.

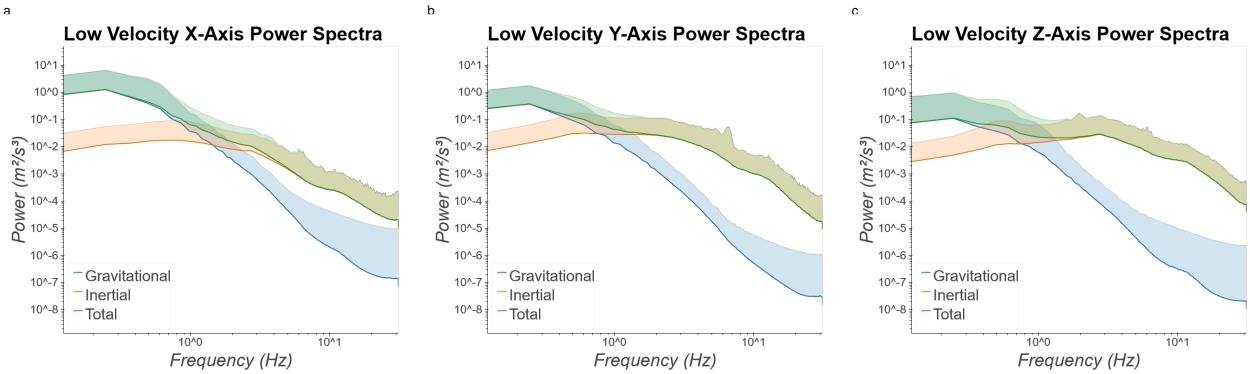

Supplemental Figure S1. Power spectra calculated from gravitational (blue), inertial (orange), and sum total linear acceleration (green) during low velocity (<0.75 m/s) epochs along X- (S1a), Y- (S1b), and Z-axes (S1c). Figure axes are log-scaled. Approximate crossing points in relative power between gravitational and inertial acceleration are observed at 1.455 Hz, 0.77 Hz, and 0.758 Hz for X-, Y-, and Z-axes, respectively.

Low and High Velocity Head Orientation

In addition to measuring head roll and head pitch across all participants and velocities, we measured head roll and head pitch across all participants during low- and high-velocity epochs. Given the proportion of total data that are comprised of low-velocity epochs (92.25% of all data), group-level distributions of head orientation as well as group-level KDEs of head roll and pitch look similar to their analogues across all data (Figure 2, main text). Conversely, the high-velocity head orientation distribution as well as high-velocity KDEs of head roll and pitch qualitatively differ from those measured across all velocity epochs (Fig. S4a). With respect to head roll, there appeared to be greater weight in the tails of the KDE relative to the KDE generated for roll across all velocities (Fig. S4b). Head pitch during high-velocity epochs appeared to be shifted further downward relative to head pitch across all velocities, both at a group and individual level (Fig. S4c). As high-velocity epochs primarily locomotion, this downwards shift is likely driven by concordant gaze-down behavior which functions to visually identify stable footholds[8,9].

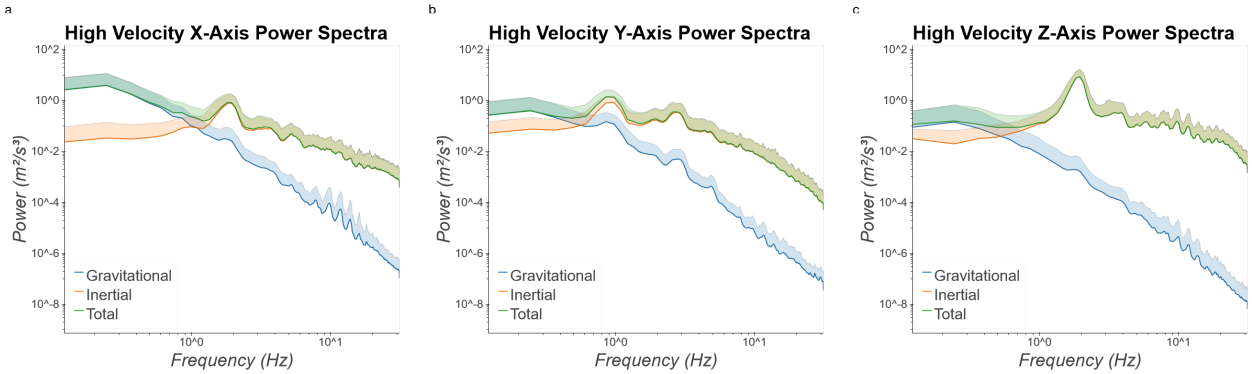

Supplemental Figure S2. Power spectra calculated from gravitational (blue), inertial (orange), and sum total linear acceleration (green) during high velocity (≥0.75 m/s) epochs along X- (S2a), Y- (S2b), and Z-axes (S2c). Figure axes are log-scaled. Approximate crossing points in relative power between gravitational and inertial acceleration are observed at 1.101 Hz, 0.566 Hz, and 0.525 Hz for X-, Y-, and Z-axes, respectively.

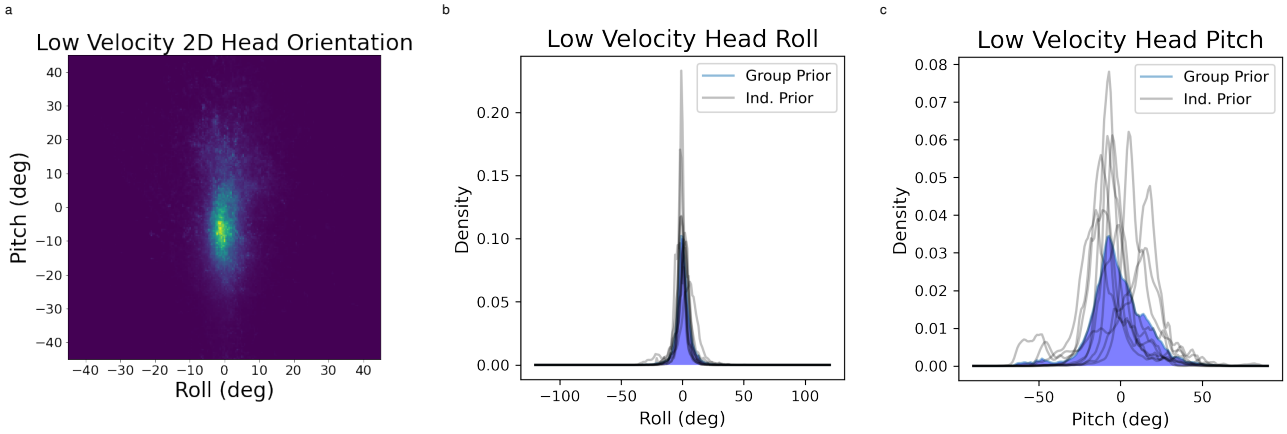

Supplemental Figure S3. 2D head orientation measured across all participants during low-velocity epochs. Marginal kernel density estimates (KDEs) for roll and pitch during low-velocity epochs are also plotted. The KDEs plotted in blue represent the distributions across all participants, while black traces represent KDEs for individual participants.

Moments of Low and High Velocity Head Orientation

We also calculated moments of pitch and roll KDEs during low and high-velocity epochs across all participants. Descriptions of these moments as well as formulae used to calculate them can be found in Table S1. In general, these low-velocity KDEs resembled KDEs generated from both low- and high-velocity epochs. During low-velocity epochs, pitch was slightly biased downward (μ_1 = -1.574°) while average roll was closer to zero (μ_1 = 0.475°). Pitch had much higher variance (μ_2 = 288.39°) than roll (μ_2 = 39.673°). Both pitch (μ_3 = -0.036) and roll (μ_3 = 0.144) had little skewness during low-velocity epochs, while roll (μ_4 = 7.297) had greater excess kurtosis than pitch (μ_4 = 1.808).

KDEs generated from high-velocity data looked qualitatively different from KDEs generated from both low- and high-velocity data. In particular, pitch appeared to show greater downward bias relative to the pitch KDE generated from all data. For high-velocty epochs, both roll (μ_1 = 1.832°) and pitch (μ_1 = -4.418°) were more biased away from upright. Pitch (μ_2 = 208.98°) continued to show higher variance than roll (μ_2 = 23.85°), and both pitch (μ_3 = 0.331) and roll (μ_3 = 0.02) showed low levels of skewness. Roll (μ_4 = 4.028) measured during these epochs continued to have higher excess kurtosis than pitch (μ_4 = 0.143).

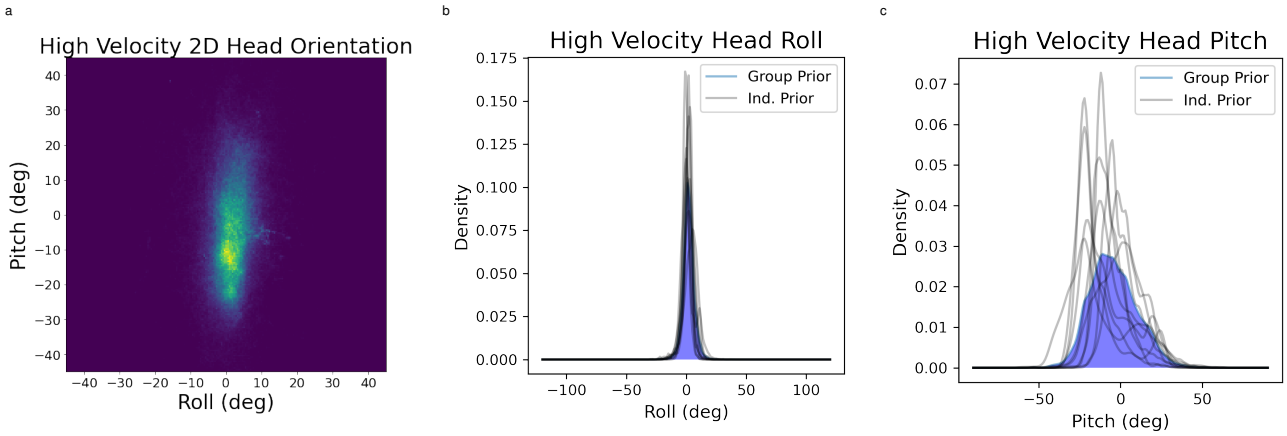

Supplemental Figure S4. 2D head orientation measured across all participants during high-velocity epochs. Marginal kernel density estimates (KDEs) for roll and pitch during high-velocity epochs are also plotted. The KDEs plotted in blue represent the distributions across all participants, while black traces represent KDEs for individual participants.

Moment	**Description**	**Formula**	**Low Vel. Roll**	**Low Vel. Pitch**	**High Vel. Roll**	**High Vel. Pitch**
Mean	The sum of a set of numbers divided by the count of that set.	$\mu_1 = \frac{1}{n}\sum_{i=1}^{n}$	0.475	-1.574	1.832	-4.148
Variance	The extent to which a set of numbers is spread out from the mean.	$\mu_2 = \frac{\sum_{i=1}^{n}(x_i - \bar{x})^2}{n-1}$	39.673	288.39	23.85	208.98
Skewness	The extent to which a given distribution is asymmetrical or otherwise lopsided.	$\mu_3 = \frac{m_3}{m_2^{3/2}}$ where $m_i = \frac{1}{N}\sum_{n=1}^{N}(x[n] - \bar{x})^i$	0.144	-0.036	0.02	0.331
Kurtosis	The weight of a given distribution's tails.	$\mu_4 = \frac{m_4}{m_2^{4/2}} - 3$ where $m_i = \frac{1}{N}\sum_{n=1}^{N}(x[n] - \bar{x})^i$	7.297	1.808	4.028	0.143

Supplemental Table S1. Descriptions, formulae, and values for first four central moments used to describe low-velocity and high-velocity pitch and roll kernel density estimates. Moments are calculated from group-level data plotted in blue in Figs. S3b, S3c, S4b, and S4c.

References

1. MacNeilage, P. R., Ganesan, N. & Angelaki, D. E. Computational approaches to spatial orientation: From transfer functions to dynamic bayesian inference. *J. Neurophysiol.* **100**, 2891–2996 (2008).

2. Scott, D. W. *Multivariate Density Estimation: Theory, Practice and Visualization* (John Wiley & Sons, Inc., New York, New York, United States of America, 1992).

3. Vingerhoets, R. A. A., Medendorp, W. P. & van Gisbergen, J. A. M. Body-tilt and visual verticality perception during multiple cycles of roll rotation. *J. Neurophysiol.* **99**, 2265–2280 (2008).

4. de Vrijer, M., Medendorp, P. & Van Gisbergen, J. A. M. Accuracy-precision trade-off in visual orientation constancy. *J. Vis.* **9**, 1–15 (2009).

5. Schöne, H. On the role of gravity in human spatial orientation. *Aerosp. Medicine* **35**, 764–772 (1964).

6. Cohen, M. M. & Larson, C. A. Human spatial orientation in the pitch dimension. *Percept. Psychophys.* **16** (1974).

7. MacDougall, H. G. & Moore, S. T. Marching to the beat of the same drummer: The spontaneous tempo of human locomotion. *J. Appl. Physiol.* **99**, 1164–1173 (2005).

8. Matthis, J. S., Yates, J. L. & Hayhoe, M. M. Gaze and the control of foot placement when walking in natural terrain. *Curr. Biol.* **28**, 1224–1233.e5 (2018).

9. Pelz, J. B. & Rothkopf, C. Chapter 31 - oculomotor behavior in natural and man-made environments. In Van Gompel, R. P., Fischer, M. H., Murray, W. S. & Hill, R. L. (eds.) *Eye Movements*, 661–676 (Elsevier, Oxford, 2007).